Spectroscopic characterization of laser-induced tin plasma

S. S. Harilal,[a)] Beau O'Shay, and Mark. S. Tillack
*Center for Energy Research, University of California San Diego, 9500 Gilman Drive,
La Jolla, California 92093-0438*

Manoj V. Mathew
International School of Photonics, Cochin University of Science and Technology, Cochin 682022, India

Optical emission spectroscopic studies have been carried out on a tin plasma generated using 1064-nm, 8-ns pulses from a Nd:yttrium aluminum garnet laser. Temperature and density were estimated from the analysis of spectral data. The temperature measurements have been performed by Boltzmann diagram method using singly ionized Sn lines, while density measurements were made using the Stark broadening method. An initial temperature of 3.2 eV and density of 7.7 $\times 10^{17}$ cm^{-3} were measured. Temporal and spatial behaviors of electron temperature and density in the laser-generated tin plasma have been analyzed. Time evolutions of density and temperature are found to decay adiabatically at early times. The spatial variation of density shows approximately $1/z$ dependence. The time-integrated temperature exhibits an appreciable rise at distances greater than 7 mm. This may be caused by the deviation from local thermodynamic equilibrium at larger distances from the target surface. © *2005 American Institute of Physics.* [DOI: 10.1063/1.1977200]

I. INTRODUCTION

Laser-produced plasma is one of the most promising options in the development of a light source for next-generation extreme ultraviolet (EUV) lithography.[1] Transient laser-produced tin plasma is currently considered as a candidate for an EUV radiation source. Spitzer *et al.*[2] studied Sn as an efficient target to convert Nd:YAG (yttrium aluminum garnet) radiation to 13.5-nm EUV radiation, achieving over 2% conversion efficiency. Laser-induced plasma (LIP) techniques are also used in space applications such as in chemical sensors for the exploration of Mars and micropropulsion for satellite positioning, as well as in the detection of biological molecules.[3,4] Other important applications of LIP include pulsed laser deposition,[5] nanoparticle and cluster production,[6,7] and laser-induced breakdown spectroscopy (LIBS).[8]

Laser-created plasma characteristics are strongly dependent upon several key parameters, including laser intensity, pulse duration and wavelength, target material and geometry, and the nature and pressure of any ambient gas. The plasma characteristics also vary with distance from the target surface, as well as with time following the onset of plume formation.[9] Several diagnostic tools can be employed for measuring plume parameters including optical emission spectroscopy (OES), laser-induced fluorescence (LIF), laser absorption spectroscopy (LAS), interferometry, mass spectrometry, beam deflectometry, etc.[10,11] OES is one of the simplest, nonintrusive ways to investigate early plasma dynamics since it uses intrinsic light emission from the LIP and does not require external excitation. This advantage makes the OES experimental setup very simple and adaptable to automation and remote sensing. Using OES one can obtain fundamental information about the plume by looking directly

at the emission spectrum. Spectral information in its most sophisticated form can provide information on the plasma ionization balance, rate processes, and the densities and temperatures. However, estimation of different parameters of the plume using OES requires some assumptions, most importantly of which is the existence of local thermodynamic equilibrium (LTE) and optically thin plasma. Recently, OES was utilized for investigating the effect of an ambient gas[12] and magnetic field[13] on an expanding, laser-produced plasma.

Most of the previous studies of fully dense tin targets focused upon the EUV emission,[14] while little effort has been spent in understanding the dynamics and evolution of laser-created Sn plasma in the visible regime. It is extremely important to understand the evolution of excited neutral and ionized species since these will act as debris in a tin plasma-based EUV source. Moreover, little attention has been paid to characterizing the tin plume, particularly in estimating fundamental quantities such as electron temperature, electron density, and their evolution after plasma ignition. In the present paper we document the evolution and dynamics of laser-generated Sn plasma employing optical emission spectroscopy. Spatially and temporally resolved emission spectra were measured in the early stage of plasma decay. We estimated the most important parameters of the plasma, viz., electron density (n_e) and temperature (T_e) along with their temporal evolution at various locations in the plasma. This will provide much physical insight into the complex mechanisms involved in the laser-matter and laser-plasma interactions. The Stark broadening method was used for the determination of electron density, and Boltzmann plot was used to calculate the electron temperature by assuming LTE conditions. For spatial analysis of the plume, time-integrated spectral lines were used and the plasma parameters were measured up to 16 mm from the target surface.

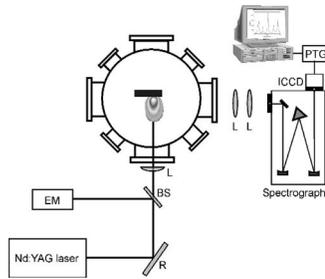[a)]Electronic mail: sharilal@ucsd.edu

FIG. 1. Schematic of the experimental setup used for optical emission spectroscopic studies. (EM, energy monitor; R, reflector; BS, beam splitter; L, lens; PTG, programmable timing generator; and ICCD, intensified CCD camera.)

II. EXPERIMENTAL SETUP

We have performed time- and space-resolved spectroscopic analyses for estimating the temperature and density of the tin plasma. A schematic of the experimental setup is given in Fig. 1. 1064-nm, 8-ns [full width at half maximum (FWHM)] pulses from a Nd:YAG laser operated at 10 Hz was used to create tin plasma in a stainless-steel vacuum chamber. The vacuum chamber was pumped using a cryogenic pump and a base pressure of $\sim 10^{-6}$ Torr was easily achieved. A 2-mm-thick tin target in the form of a slab was translated to provide a fresh surface to avoid errors associated with local heating and drilling. The laser beam was focused onto the target surface at normal incidence using an $f/12$ antireflection-coated planoconvex lens. The beam energy was monitored using a thermal surface absorbing energy meter (Ophir, Model 30A). The plasma plume was produced with a laser intensity ~ 2 GW/cm^2.

The light emitted from the luminous plasma was transmitted though a quartz window mounted orthogonally to the direction of plume expansion. An optical system was used to image the plasma plume onto the entrance slit of a 0.5-m Czerny-Turner spectrograph (Acton Pro, Spectra-Pro 500i) so as to have one-to-one correspondence with the sampled area of the plume and the image. The optical system was translated to monitor the different parts of the plume. The exit port of the spectrograph was coupled to an intensified charge-coupled device (CCD) camera (ICCD, PI MAX Model 512 RB) that was operated with vertical binning of the CCD array to obtain spectral intensities versus wavelength. A programmable timing generator was used to control the delay time between the laser pulse and the detector system with an overall temporal resolution of 1 ns. The spectrograph was equipped with three gratings: 150, 600, and 2400 g/mm. The effective dispersion with 150, 600, and 2400 grooves/mm was 12.6, 3.1, and 0.6 nm/mm, respectively. For the plasma temperature measurement the spectral details of the plume were collected using the 600-grooves/mm grating, and for Stark broadening studies the holographic grating with 2400 grooves/mm was used. The recorded maximum resolution of the spectrograph with the 2400-g/mm grating with a frequency-stabilized He–Ne laser was ~ 0.025 nm. The spectral response calibration of the system (spectrograph and detector) was performed using a tungsten lamp for the wavelength range of 350–800 nm.
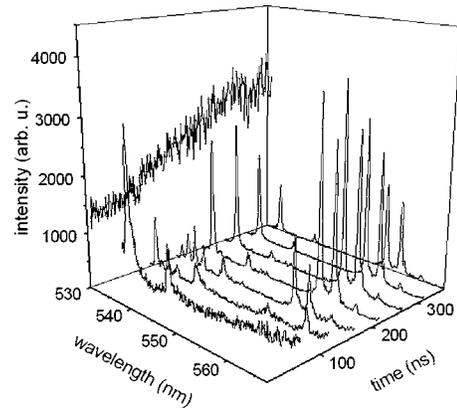

FIG. 2. Time-resolved emission spectra from laser-produced tin plasma. The spectra were recorded at a distance of 1 mm from the target surface and the gate time of the intensifier was set at 20 ns. Most of the emission lines in the figure are due to singly charged tin ions.

III. RESULTS AND DISCUSSION

The laser ablation process can be classified into three regimes: evaporation of the target material, interaction of the evaporated cloud with incident laser beam resulting in cloud heating and plasma formation, and expansion and rapid cooling of the plasma. The dynamic, transient behavior of the LIP is challenging for diagnostics since the fundamental plasma quantities vary dramatically in time and space. We performed spatial and temporal analyses of visible emission from the laser-produced tin plume. Observations were made of the plasma created by the interaction of the laser beam with the target in a direction perpendicular to that of the laser beam.

For recording the time-resolved spectra, the gate of the intensifier was set to 20 ns. Typical emission spectra of the laser-produced Sn plasma at different times after the peak of the laser pulse are given in Fig. 2. As seen in the figure during the initial stages, especially <60 ns, continuum emission dominates the spectral line emission, making OES inadequate for diagnosing the plume. As time evolves, the line-to-continuum ratio increases. The continuum radiation, or bremsstrahlung, occurs when a free electron collides with another particle and makes a transition to another free state of lower energy, with the emission of a photon. In a plasma that is sufficiently hot, most of the atoms are stripped of their orbital electrons, hence making electron-ion recombination and bremsstrahlung the dominant emission mechanisms. This situation typically occurs for electron temperatures on the order of a few eV. With time, the line-to-continuum ratio increases and finally, the spectrum consists of mainly ionic and atomic lines. At shorter time delays, ionic species are predominant, but for time delays exceeding 200 ns, excited atomic emissions are evident. The spectral details showed at early times that most of the emission from the tin plume was contributed by singly charged ions. At later times some excited neutral species were observed.

A. Time of flight and velocity

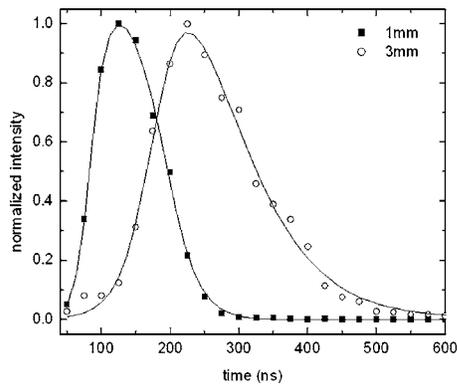Time-and space-resolved OESs of LIP species at various distances from the target could be used to estimate the

FIG. 3. Time-of-flight profile of the Sn$^+$ ion at 556.2 nm obtained from spectral data is given for two distances from the target surface. The expansion velocity of the species is obtained from this plot. The solid points in the plot represent the experimental data and the solid curves represent the best fit.

FIG. 4. Stark-broadened profiles of Sn$^+$ lines at 645.4 nm at different distances from the target surface. The smooth curves represent the fitted Lorentzian profiles.

plasma expansion rate near the target. The temporal evolution of spectral line intensity at a constant distance can be used to construct the time-of-flight (TOF) profile. TOF studies of the plasma provide vital information regarding the time taken for a particular species to evolve after the plasma has formed. Specifically, this technique gives details of the velocity of the emitted particles. This procedure for determination of plasma velocity should be used with care due to the superposition of both expansion and forward movements of the plasma plume. Moreover, the procedure does not take into account the different populations or origins of the same species. In a LIP, it has been observed that the propagation velocity of a particular species depends upon its charge state. The expansion velocities of the ionized species are found to increase with degree of ionization, while excited neutral species and molecules are the slowest moving particles.[15] Figure 3 shows a normalized TOF profile of Sn$^+$ species at 556.2 nm in vacuum. From the temporal shift of the TOF peaks at sequential spatial points, it is possible to obtain the mean velocity of the LIP along the propagation axis. The estimated expansion velocities of Sn$^+$ species at distances of 1 and 3 mm from the target surface are 0.81×10^6 and 1.3×10^6 cm/s, respectively. The estimated expansion velocity for excited neutral tin species at 3 mm from the target is 4.5×10^5 cm/s, showing that neutrals are moving much slower than ions. The expansion velocities of the species are found to increase with a distance from the target surface. This trend in the LIP velocity has been reported previously, and is due to the initial acceleration of the ablated particles from zero velocity (before the laser-pulse energy reaches the ablation threshold), to a maximum velocity.[16]

B. Density measurement using Stark broadening

The shape and width of the spectral lines emitted by a plasma are governed by collisional processes perturbing the emitting atoms and ions. We have selected the line-broadened profile of the Sn$^+$ line at 645.4 nm ($6p^2P^0 \rightarrow 6s^2S$) for the density measurements. The main mechanisms contributing to the broadening of the spectral lines are Stark, resonance, Doppler, and instrumental broadening. The
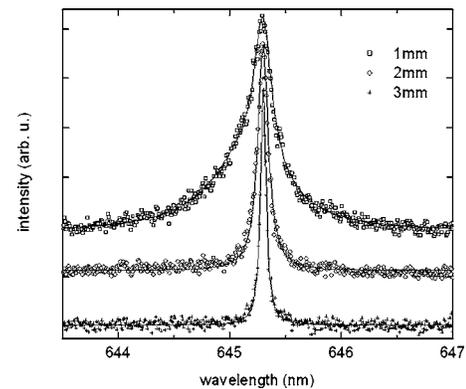
effect of resonance broadening is proportional to the ground-state number density and the transition oscillator strength. For ablation in vacuum, where ablated species exhibit high expansion velocities, one of the dominant contributions to the spectral line broadening is Doppler broadening. This is due to Doppler shifts (i.e., $\Delta\lambda_D = \lambda v_z/c$) experienced by the various species in the plume exhibiting different velocity components v_z in the direction of observation. Since the expansion velocities of the Sn$^+$ ions are found to be on the order of 10^6 cm/s which corresponds to a Doppler linewidth FWHM of ~ 0.02 nm, the effect due to Doppler broadening may be safely neglected. Setting the spectrograph at its maximum resolution can minimize the instrumental broadening. Stark broadening of spectral lines in plasmas is caused by collisions of charged species, resulting in both a broadening of the line and a shift in the peak wavelength. The FWHM of a Stark-broadened line (in angstroms) without an ionic contribution is given by the simple relation[17]

$$\Delta\lambda_{1/2} = 2W\left(\frac{n_e}{10^{16}}\right) \text{Å}, \tag{1}$$

where W is the electron-impact parameter which can be selected for different temperatures.[17] The impact parameters of the 645.4-nm Sn$^+$ line are obtained from Ref. 18 for two temperatures, viz., 0.86 and 2.86 eV. The uncertainties in the impact parameters are within 50% for 0.86 eV and within 40% for 2.86 eV.[18] We estimated the density of the plasma by assuming the impact parameters would vary linearly in the temperature range mentioned above. Typical Stark-broadened profiles of Sn$^+$ lines recorded at different distances from the target are given in Fig. 4. Stark-broadened line profiles are approximately Lorentzian and the experimental curves shown here in Fig. 4 fit fairly well with a typical Lorentzian profile.

C. Temperature measurement

The most widely used method in determining the temperature of laser-induced plasmas is Boltzmann plot technique. Using the intensity of line emission from a single species, it provides the excitation temperature of the plasma.[19,20] In its simplest form, only two emission lines are necessary to obtain the excitation temperature, provided
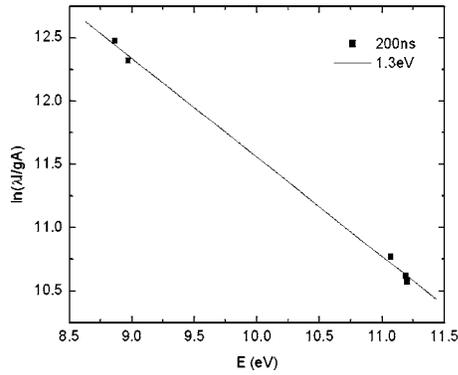
FIG. 5. Typical Boltzmann plot used for estimating temperature of the plasma. Emission lines from singly ionized tin species are used for obtaining the Boltzmann plot.

FIG. 6. The temporal evolution of density at different distances from the target surface.

there is sufficient difference between their upper energy levels. Boltzmann plot, however, uses several emission lines, thus providing a more accurate estimate of electron temperature. A linear fit to experimental data not only validates the assumption of a Maxwellian electron distribution, but serves as a check for errors in line assignment or transition probability value.[19] A second method used to obtain the plasma temperature is based on the Saha equation. This combines the number densities of consecutive ionization stages of a gas with their Maxwell-Boltzmann factor, resulting in the population distribution for each constituent species. In the present experiment, the plasma electron temperature was deduced from the Boltzmann plot method. If the plasma is assumed to be in LTE, the Boltzmann distribution can be used to estimate the population of the excited state and is written as[17]

$$n_{nm} = n_n \frac{g_m}{Z} e^{-E_m/kT}, \qquad (2)$$

where n_{nm} is the population of the mth excited level; g_m, the statistical weight of the upper level of the transition; E_m, the excitation energy; k, Boltzmann's constant; and T, the temperature. The emission intensity of a line is related to the population of the excited level through the following relation

$$I_{nm} \approx A_{nm} n_{nm} \frac{hc}{\lambda_{nm}} = A_{nm} n_n \frac{g_m hc}{Z\lambda_{nm}} e^{-E_m/kT}, \qquad (3)$$

where A_{nm} is the atomic transition probability and λ_{nm} is the wavelength of the line. For a LTE plasma, a plot of $\ln(I\lambda/Ag)$ against E for several spectral lines should be a straight line of slope $-1/kT$. The plasma temperature was estimated from the Boltzmann plot of 684.4 nm ($6p^2P^0 \rightarrow 6s^2S$), 645.4 nm ($6p^2P^0 \rightarrow 6s^2S$), 559.0 nm ($4f^2F^0 \rightarrow 5d^2D$), 556.2 nm ($6d^2D \rightarrow 6p^2P^0$), and 533.2 nm ($6d^2D \rightarrow 6p^2P^0$) line intensities of Sn+ for which absolute transition probabilities are well known. The energy levels, transition probabilities,[21,22] and lifetimes[23] of singly ionized Sn are well documented in recent articles. The uncertainties in the transition probability values are ±25%.[24] A typical Boltzmann plot used for calculating the temperature is given in Fig. 5. All the data exhibited a linear fit with a correlation coefficient better than 0.98.
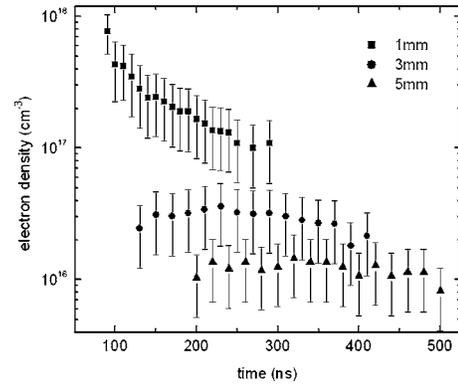
The measurement of temperature and density using spectral line intensities and broadening requires the use of optically thin sources to avoid self-absorption effects. We assumed that the plasma was optically thin for the lines considered for temperature and density estimations. The effect of self-absorption depends on the parameters that are characteristic of a particular line including oscillator strength, level energies, and degeneracies, as well as on plasma quantities such as density and temperature. The resonance lines are most affected by self-absorption because of the high population of lower levels and large oscillator strengths. An estimate of the upper limit on the absorption coefficient for the spectral lines used in temperature and density estimations showed self-absorption to be negligible.[25] In addition, all of these lines originate at high-lying levels and terminate in excited levels, making them optically thin. This is also evidenced by the fact that the branching ratio of various spectral lines at different times of plume evolution showed no variation. Moreover, in a LIP expansion into vacuum, the ejected plasmas have highly directed kinetic energies as well as steep velocity and density gradients, all of which will reduce the effective optical depth appreciably.

D. Temporal evolution of temperature and density

The temporal evolution of electron temperature and electron density is of prime importance since many kinetic reaction rates depend directly or indirectly on these parameters. We studied the temporal evolution of plume parameters at different distances from the target surface. Figures 6 and 7 show the temporal evolution of density and of temperature of tin plasma recorded at 1, 3, and 5 mm from the target surface. The errors provided for density and temperature measurements considered the uncertainty in the impact parameters,[18] transition probabilities,[24] and the experimental error. At shorter times, the line-to-continuum ratio is very small and the temperature measurement is very sensitive to errors in setting the true continuum level. This problem is particularly acute for times up to ~60 ns. For times >60 ns, the line-to-continuum ratio is within a reasonable limit, and interference with the continuum measurement is not severe. Therefore, the values of n_e and T_e shown in the figures are reliable. For the temperature and density measurements the
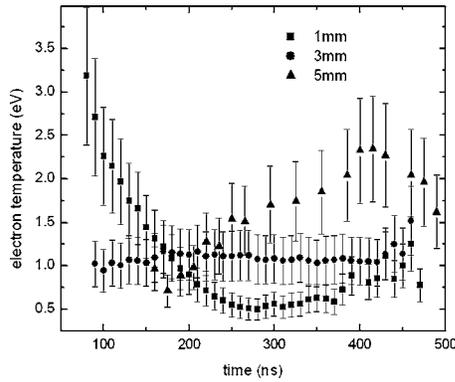
FIG. 7. The temporal evolution of temperature at different distances from the target surface.

FIG. 8. Time-integrated density as a function of distance from the target surface.

gate width of the intensifier was set to 20 ns. It is evident from the figures that the density and temperature attain their peak values close to the target surface, and then decrease due to the expansion of the plume. An initial electron temperature of about 3.2 eV and a density of 7.7×10^{17} cm^{-3} are observed at 1 mm from the target. Initially, the plasma expands isothermally during the laser pulse. After termination of the pulse, no more energy is pumped into the plasma, and both the temperature and density decrease rapidly with time. Thermal energy is converted into directed kinetic energy, and the plasma cools through adiabatic expansion. According to an adiabatic expansion model, the density and temperature should follow, respectively, a t^{-3} and t^{-2} dependence with time t. The temperature is found to exhibit approximately t^{-2} dependence at 1 mm from the target surface, which is consistent with an adiabatic expansion.

Observations show a higher rate of decay of density at 1 mm than for 3 or 5 mm from the target. For example, at 1 mm the density drops from 7.7×10^{17} to 1.6×10^{17} cm^{-3} within 200 ns of plasma evolution, while at 3 mm, the density slightly increases at earlier times and only drops at later times. It can be seen from Fig. 7 that, similar to the density variation with time, the electron temperature decreases rapidly at 1 mm from the target surface. Within 200 ns of plume evolution, the temperature at 1 mm decays from 3.2 to 0.5 eV. A slight increase in temperature with time is noted at later times at 1 mm. A weak dependence of temperature on time is observed at 3 mm from the target surface. The temperature is almost constant around 1 eV at this distance. It can be seen from Fig. 7 that the electron temperature is significantly larger at later times. This is more noticeable at 5 mm from the target surface where temperature is found to be an increasing function of time up to 400 ns. One source of electron temperature increase is the laser energy absorption through inverse bremsstrahlung that occurs during the laser-plasma interaction. The increase in plasma temperature is most likely due to energy released through recombination, which compensates the expansive cooling. Since the density of the plume is $\geqslant 10^{16}$ cm^{-3}, the three-body recombination will eventually dominate radiative recombination. In three-body recombination the electron is initially captured into an upper excited level and then cascades down to the ground state either through radiative transitions or by transferring
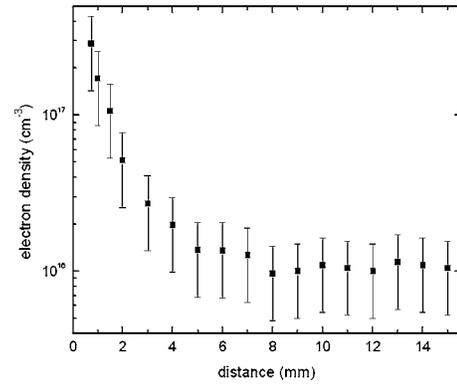
energy to free electrons in collisions. Three-body recombination becomes important when the thermal energy of the free electrons has fallen to much less than the ionization energy. In this situation a very small three-body recombination rate can lead to sufficient transfer of energy to the electrons to make a large change in the electron temperature decay rate without affecting the density decay rate. This will effectively reduce the cooling rate caused by adiabatic expansion. A rise in temperature with time at larger distances was also noted by Gordillo-Vazquez *et al.*[26] for a laser-produced LiNbO$_3$ plume and was explained by atom-atom collisions at greater distances from the target.

E. Spatial dependence of temperature and density

We observed an increase in temperature with time for tin plumes that became especially noticeable at larger distances from the target. In order to gain a better understanding of the spatial behavior of the plume, spectral measurements were made at sequential distances from the target surface (up to 16 mm). Spectral and line-shape analyses were repeated at different distances from the target. This provided details about the evolution of electron temperature and density in space as well as insight into the basic ionization processes occurring in the pulsed laser ablation. In a laser-produced plasma species with different charge states propagate with different velocities. This behavior is more relevant at larger distances from the target surface where all species begin to separate out in time. In order to compensate this phenomenon, we selected a large gate width (1 μs) for doing the spatial analysis of the plume, where the gate was delayed for increasing separation from the target surface. Hence, temperature and density values estimated at various distances are indicative of the average local conditions rather than the defining conditions at a particular stage of the plasma's evolution.

The variation of density with distance from the target surface is given in Fig. 8. The density shows a decreasing behavior with distance. With increasing separation from the target surface, the electron density falls from 2.9×10^{17} cm^{-3} at 1 mm to 1×10^{16} cm^{-3} at 15 mm. The decay of the density is much faster at shorter distances from the target surface, especially <3 mm after which it levels off. The variation of density with distance (z) approximately follows a $1/z$ law, which indicates that the initial expansion of
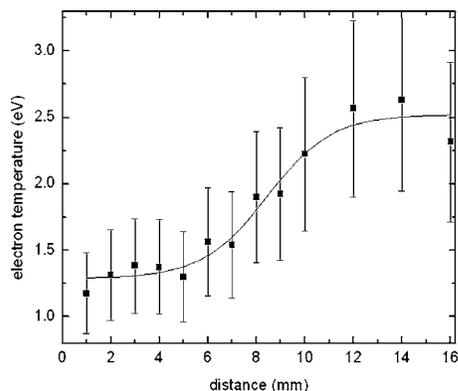
FIG. 9. The variation of temperature with distance from the target surface is given. Time-integrated spectra are used for temperature estimation. The temperature is found to increase at distances $\geqslant 6$ mm and may be caused by deviations from LTE.

the plume is one dimensional, and is in good agreement with the predictions of the plume expansion model given by Singh *et al.*[27]

The time-integrated temperature variation with distance from the target surface is given in Fig. 9. The temperature is found to be more or less constant at distances <6 mm but at greater distances the temperature is found to increase. This is contrary to what has been reported for plasmas produced by laser ablation of carbon,[28] aluminum,[13] and other targets.[26] The typical spatial variation of temperature in these laser-created plasmas was a rapid decay near the target, but at larger distances the temperature became a slowly varying function of space. The leveling off of the temperature at larger distances is mainly due to the energy gained from three-body recombination that compensates the expansive cooling. In the present studies, the temperature is found to increase for distances greater than 5 mm. This is also consistent with our time-resolved temperature measurements where we noted an appreciable temperature increase at later times. In plasmas three-body recombination heating occurs through the release of the ionization energy as electrons and ions recombine. This process is generally observed for plasma temperatures on the order of 1 eV. It was noted that the three-body recombination rate coefficient strongly depended on the nature of the ambient gas used.[29] Gordillo-Vazquez *et al.*[29] estimated the ionization rate coefficient and three-body recombination rate coefficient for laser-produced lithium niobate plasma and found these values to vary with distance for different ambient gases. Compared to the expansion into a vacuum, the interaction of the plume with an ambient gas is a far more complex gas dynamic process that involves deceleration, attenuation, thermalization of the ablated species, confinement, formation of shock waves, etc.[12] The observed temperature and density in this experiment favor three-body recombination. However, in the present experiment where the plume expands freely into vacuum, the efficiency of this process will be reduced. When the plasma expands into vacuum, the plume species move with different expansion velocities. It is well known that species with higher charge states propagate much faster than their less-ionized counterparts and neutrals. Therefore, at larger distances where the

differential expansion becomes noticeable, the various species will become separated out and collide less frequently with one another. This will reduce the rate of temperature equilibration and cooling, and perhaps violate the assumption of local thermodynamic equilibrium in the plasma.

We have considered the plasma to be in LTE in the estimation of temperature from spectral data. The issue of LTE in laser-produced plasmas has been discussed by several authors.[17,30,31] In a transient system, such as a plasma formed by a pulsed laser source, the existence of LTE requires that the electron-atom and electron-ion collisional processes occur sufficiently fast and dominate radiative processes. In a system that is in LTE, particles will have Maxwellian velocity distributions, population levels will be distributed according to Boltzmann's statistics, ionization states will be described by Saha's equation, and the radiation density will obey Planck's law. In the present experiment we believe that the plume is in LTE because of the following facts. The Boltzmann plot, which is used for estimating the temperature from line intensities of various Sn^+ lines showed a straight line fit with high correlation value. We confirm the validity of the McWhirter criterion[32] in the present experiment, which states that the minimum density for LTE should be

$$n_e \geqslant 1.4 \times 10^{14} T_e^{1/2} (\Delta E)^3 \text{ cm}^{-3}, \qquad (4)$$

where T_e and ΔE (the energy difference between the upper and lower energy levels) are in eV. For the transition with the largest energy-gap $\Delta E = 2.325$ eV, applying the peak plume temperature of 3.2 eV to this criterion predicts a lower limit for n_e of 3.15×10^{15} cm^{-3}. Our observed values of n_e are always greater than this lower bound, implying that the LTE approximation assumed for our analysis is valid. These are necessary conditions for LTE, but not sufficient. At larger distances and greater times, the number densities of the plasma are low and the movement of the boundary region is rapid, so LTE is probably not a good assumption. This is supported by the fact that the time-integrated density dropped to 1×10^{16} cm^{-3} which is considerably lower than the measured initial density values obtained from time-resolved studies ($\sim 7 \times 10^{17}$ cm^{-3}). The large drop in density will affect the thermal equilibrium established between the upper levels of Sn^+ ions used for the Boltzmann plot. Therefore we conclude that LTE may not be a good approximation for large distances and late stages of plasma evolution.

IV. SUMMARY

Optical emission spectroscopy is used to characterize the laser-produced plasma from tin in vacuum. Time-and space-resolved measurements of electron density and temperature have been carried out using emission lines of singly ionized tin. Line intensities from the same ionization stage of tin species were used in the Boltzmann plot for determining electron temperature, and the Stark-broadened profiles of first ionized tin species were used to calculated the electron density. At earlier times, especially below 60 ns the intense continuum radiation is dominant, making it difficult to extract line intensities and profiles. The line-to-continuum ratio increases as time evolves. An initial temperature of 3.2 eV

and density of 7.7×10^{17} cm^{-3} were measured. In the early stage of plasma evolution, the electron temperature and density rapidly decrease which is characteristic of an adiabatic expansion. The density is found to decay much slower at larger distances from the target. At later times, a rise in temperature is observed that becomes more evident at 5 mm from the target surface. Measurements of the spatial variation of temperature and density were carried out using time-integrated intensities from tin ion lines. The density approximately followed a $1/z$ dependence on distance, which is consistent with an adiabatic expansion. The temperature near the target was more or less constant, but increased significantly for distances greater than 7 mm. A deviation from the assumption of LTE for temperature estimation may be the source of this rise in temperature at larger distances.

[1] B. Marx, Laser Focus World **39**, 34 (2003).

[2] R. C. Spitzer, R. L. Kauffman, T. Orzechowski, D. W. Phillion, and C. Cerjan, J. Vac. Sci. Technol. B **11**, 2986 (1993).

[3] J. D. Hybl, G. A. Lithgow, and S. G. Buckley, Appl. Spectrosc. **57**, 1207 (2003).

[4] A. K. Knight, N. L. Scherbarth, D. A. Cremers, and M. J. Ferris, Appl. Spectrosc. **54**, 331 (2000).

[5] *Pulsed Laser Deposition of Thin Films*, edited by D. B. Chrisey and G. K. Hubler (Wiley, New York, 1994).

[6] M. S. Tillack, D. W. Blair, and S. S. Harilal, Nanotechnology **15**, 390 (2004).

[7] S. Arepalli, J. Nanosci. Nanotechnol. **4**, 317 (2004).

[8] C. V. Bindhu, S. S. Harilal, M. S. Tillack, F. Najmabadi, and A. C. Gaeris, Appl. Spectrosc. **58**, 719 (2004).

[9] S. S. Harilal, C. V. Bindhu, V. P. N. Nampoori, and C. P. G. Vallabhan, Appl. Phys. Lett. **72**, 167 (1998).

[10] D. B. Geohegan, in *Pulsed Laser Deposition of Thin Films*, edited by D. B. Chrisey and G. K. Hubler (Wiley, New York, 1994), p. 115.

[11] S. Amoruso, R. Bruzzese, N. Spinelli, and R. Velotta, J. Phys. B **32**, R131 (1999).

[12] S. S. Harilal, C. V. Bindhu, M. S. Tillack, F. Najmabadi, and A. C. Gaeris, J. Appl. Phys. **93**, 2380 (2003).

[13] S. S. Harilal, M. S. Tillack, B. O'Shay, C. V. Bindhu, and F. Najmabadi, Phys. Rev. E **69**, 026413 (2004).

[14] Y. Tao *et al.*, Appl. Phys. Lett. **85**, 1919 (2004).

[15] S. S. Harilal, C. V. Bindhu, M. S. Tillack, F. Najmabadi, and A. C. Gaeris, J. Phys. D **35**, 2935 (2002).

[16] S. S. Harilal, R. C. Issac, C. V. Bindhu, V. P. N. Nampoori, and C. P. G. Vallabhan, J. Appl. Phys. **80**, 3561 (1996).

[17] H. R. Griem, *Principles of Plasma Spectroscopy* (Cambridge, New York, 1997).

[18] N. Konjevic, A. Lesage, J. R. Fuhr, and W. L. Wiese, J. Phys. Chem. Ref. Data **31**, 819 (2002).

[19] J. A. Aguilera and C. Aragon, Spectrochim. Acta, Part B **59**, 1861 (2004).

[20] J. A. Aguilera and C. Aragon, Appl. Surf. Sci. **197**, 273 (2002).

[21] T. Wujec and S. Weniger, J. Quant. Spectrosc. Radiat. Transf. **18**, 509 (1977).

[22] A. Alonso-Medina and C. Colon, Phys. Scr. **61**, 646 (2000).

[23] R. M. Schectman, S. Cheng, L. J. Curtis, S. R. Federman, M. C. Fritts, and R. E. Irving, Astrophys. J. **542**, 400 (2000).

[24] A. Alonso-Medina, C. Colon, and C. Rivero, Phys. Scr. **71**, 154 (2005).

[25] B. Martinez and F. Blanco, J. Phys. B **32**, 241 (1999).

[26] F. J. Gordillo-Vazquez, A. Perea, J. A. Chaos, J. Gonzalo, and C. N. Afonso, Appl. Phys. Lett. **78**, 7 (2001).

[27] R. K. Singh, O. W. Holland, and J. Narayan, J. Appl. Phys. **68**, 233 (1990).

[28] S. S. Harilal, C. V. Bindhu, R. C. Issac, V. P. N. Nampoori, and C. P. G. Vallabhan, J. Appl. Phys. **82**, 2140 (1997).

[29] F. J. Gordillo-Vazquez, A. Perea, and C. N. Afonso, Appl. Spectrosc. **56**, 381 (2002).

[30] E. Perez-Tijerina, J. Bohigas, and R. Machorro, J. Appl. Phys. **90**, 3192 (2001).

[31] O. Barthelemy, J. Margot, S. Laville, F. Vidal, M. Chaker, B. Le Drogoff, T. W. Johnston, and M. Sabsabi, Appl. Spectrosc. **59**, 529 (2005).

[32] G. Bekefi, *Principles of Laser Plasmas* (Wiley-Interscience, New York, 1976).